Graphene–Ferroelectric Hybrid Structure for Flexible Transparent Electrodes

Guang-Xin Ni,[†,‡,§] Yi Zheng,[†,‡] Sukang Bae,[⊥,#] Chin Yaw Tan,[∥] Orhan Kahya,[†] Jing Wu,[†] Byung Hee Hong,[⊥,#,*] Kui Yao,[∥] and Barbaros Özyilmaz[†,‡,§,△,*]

[†]Department of Physics, National University of Singapore, 2 Science Drive 3, Singapore 117542, [‡]NanoCore, National University of Singapore, 4 Engineering Drive 3, Singapore 117576, [§]Graphene Research Centre, National University of Singapore, 6 Science Drive 2, Singapore 117546, [⊥]SKKU Advanced Institute of Nanotechnology (SAINT) and Center for Human Interface Nano Technology (HINT), Sungkyunkwan University, Suwon 440-746, Korea, [∥]Institute of Material Research and Engineering (IMRE), A*STAR (Agency for Science, Technology and Research), 3 Research Link, Singapore 117602, [#]Department of Chemistry, Seoul National University, Seoul, 151-747, Korea, and [△]NUS Graduate School for Integrative Sciences and Engineering (NGS), National University of Singapore, Singapore 117456

ABSTRACT

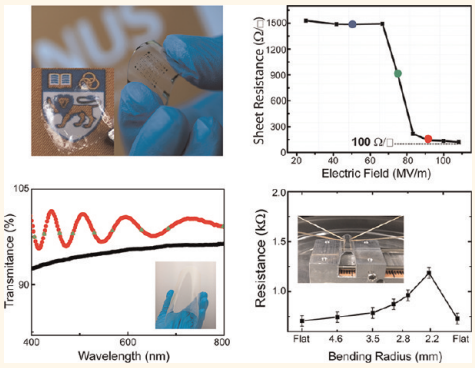

Graphene has exceptional optical, mechanical, and electrical properties, making it an emerging material for novel optoelectronics, photonics, and flexible transparent electrode applications. However, the relatively high sheet resistance of graphene is a major constraint for many of these applications. Here we propose a new approach to achieve low sheet resistance in large-scale CVD monolayer graphene using nonvolatile ferroelectric polymer gating. In this hybrid structure, large-scale graphene is heavily doped up to 3×10^{13} cm^{-2} by nonvolatile ferroelectric dipoles, yielding a low sheet resistance of 120 Ω/□ at ambient conditions. The graphene–ferroelectric transparent conductors (GFeTCs) exhibit more than 95% transmittance from the visible to the near-infrared range owing to the highly transparent nature of the ferroelectric polymer. Together with its excellent mechanical flexibility, chemical inertness, and the simple fabrication process of ferroelectric polymers, the proposed GFeTCs represent a new route toward large-scale graphene-based transparent electrodes and optoelectronics.

KEYWORDS: CVD graphene · ferroelectric polymer gating · sheet resistance · high transparency · mechanical flexibility · charged impurity scattering

Graphene keeps attracting much attention with an enormous amount of experimental and theoretical activity, since its first micromechanical exfoliation in 2004.[1–4] As a single atomic layer membrane, graphene is highly transparent (97.3%) over a wide range of wavelengths from the visible to the near-infrared (IR).[5] Owing to its covalent carbon–carbon bonding, graphene is also one of the strongest materials, with a remarkably high Young's modulus of ~1 TPa.[6] The combination of its high transparency, wideband tunability, and excellent mechanical properties make graphene a very promising candidate for flexible electronics, optoelectronics, and phonotics.[7–9] The technical breakthrough of large-scale graphene synthesis has further accelerated the use of graphene films as transparent electrodes.[10,11]

To utilize graphene as transparent electrodes for applications such as solar cells,[12] organic light-emitting diodes,[13] touch panels, and displays,[14] the key challenge is to reduce the sheet resistance to values comparable with indium tin oxide (ITO), which provides the best known combination of transparency (>90%) and sheet resistance (<100 Ω/□).[8,15] Conventional methods to reduce the sheet resistance of graphene, such as electrostatic doping, requires complex fabrication steps of dielectric deposition and gate electrode preparations, which are not practical for doping large-scale graphene and consume power to maintain the doping levels.[12,14] Chemical doping has been shown to effectively reduce the sheet resistance of graphene.[16–19] However, the doping mechanism of chemical dopants is not yet fully understood, and the relationship between charge density and carrier mobility is still under debate.[20–22] Furthermore, the adsorption of moisture and other chemical molecules after chemical treatment leads to a 40% increase of the graphene sheet resistance within a few days.[23,24] Consequently, an additional carefully chosen thin polymer coating is necessary to maintain its high conductivity without compromising its high transparency.[24] Therefore, new approaches with improved performance, zero power consumption,

* Address correspondence to barbaros@nus.edu.sg; byunghee@snu.ac.kr.

Received for review January 10, 2012 and accepted April 23, 2012.

Published online April 23, 2012
10.1021/nn3010137

© 2012 American Chemical Society

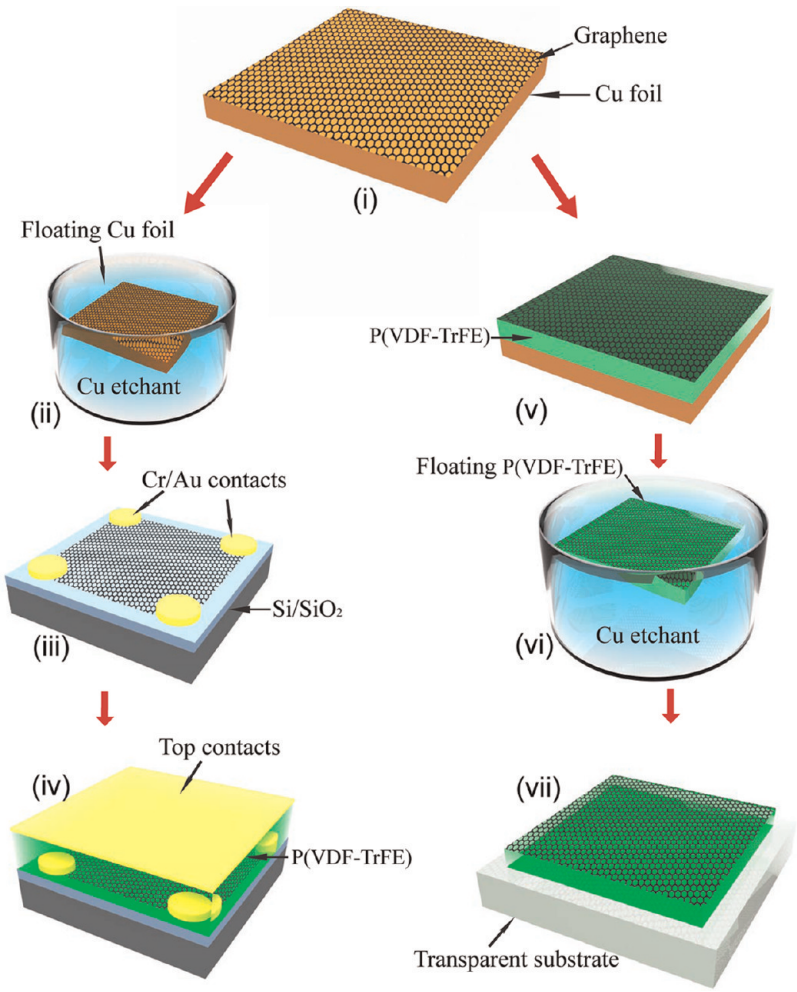

Figure 1. Schematic illustration of the GFeTC device fabrication process for both sheet resistance characterization and optical transparency measurements (see text for details). Part (i) shows the large-scale CVD graphene on a copper substrate, which is the starting point of all devices. From (ii) to (iv), device fabrications for R_S measurements are illustrated. From (v) to (vii), device fabrication of transferring a graphene−P(VDF-TrFE) hybrid structure on a transparent substrate for transmittance measurements is shown.

and simplified fabrication processes are highly desired.

Ferroelectric polymers such as poly(vinylidene fluoride-*co*-trifluoroethylene) (P(VDF-TrFE)) have been extensively explored for ultrafast, high-density, nonvolatile memories.[25−27] Recently, its potential has also been recognized for other applications, such as high-efficiency organic solar cells,[28] high-power energy storage,[29] and protective coating layer.[30] The key to many ferroelectric applications is that ferroelectric polymers can introduce a large nonvolatile doping. Also important to note is that they are chemically inert under ambient conditions. Taking graphene−ferroelectric nonvolatile memory as an example, the nondestructive and nonvolatile electrostatic doping of graphene is limited only by the remnant polarization of P(VDF-TrFE) (8 μC/cm^2), which is equivalent to a charge carrier density of 5×10^{13}/cm^2. Equally important, P(VDF-TrFE) thin films are essentially transparent (>98%) across the visible spectrum.[31] In addition, with appropriate thickness the fully polarized P(VDF-TrFE) thin films simultaneously both dope and provide excellent mechanical support to graphene. With the exception of ref 32, all previous approaches of chemically doping graphene had to be combined with a polymer supporting layer in a separate process step.[16,23] Thus, the combination of P(VDF-TrFE) with large-scale graphene provides an ideal solution for graphene for transparent conductor applications. However, to date, no experimental studies have been performed along this direction.

In this paper, we present a new route, which achieves low sheet resistance values in large-scale single-layer graphene by introducing a transparent thin ferroelectric (P(VDF-TrFE)) polymer coating. Such graphene−ferroelectric transparent conductors (GFeTCs) exhibit a low sheet resistance value down to 120 Ω/□ at ambient conditions due to a large electrostatic *nonvolatile doping* of up to 3×10^{13}/cm^2 from ferroelectric dipoles. Beyond having low sheet resistance values, the GFeTCs are also highly

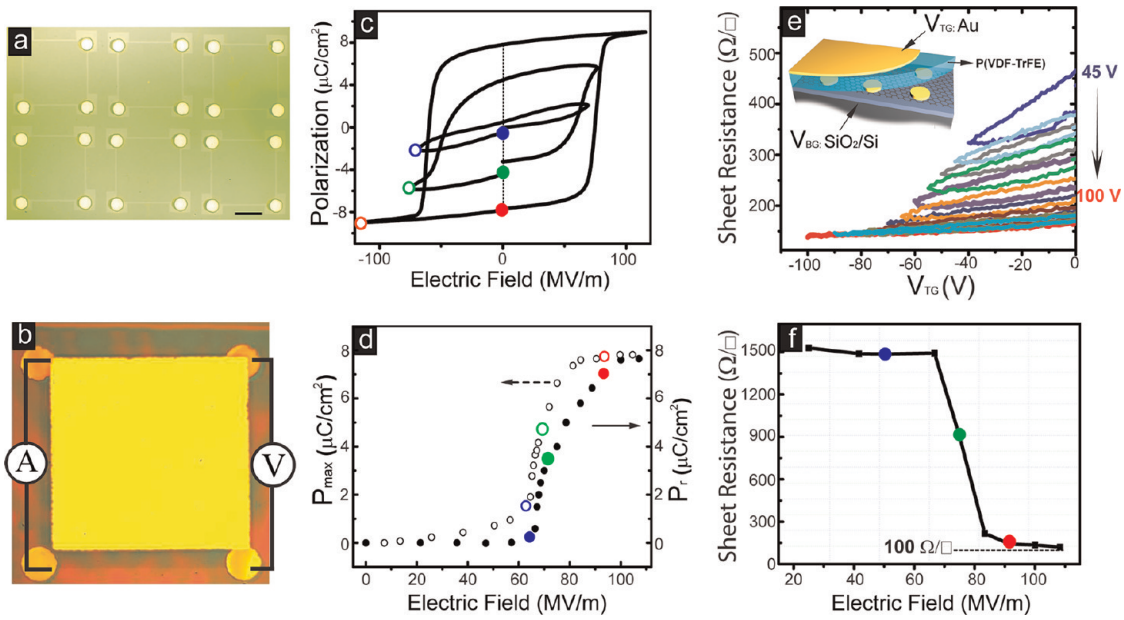

Figure 2. Devices and measurement results of R_S at ambient conditions. (a) Optical image of large-scale graphene samples with bottom contacts; the scale bar is 500 μm. (b) Optical image of a completed GFeTC device and its corresponding characterization strategy using the van der Pauw method. (c) Typical hysteresis polarization loops of our P(VDF-TrFE) ferroelectric dielectric. The solid balls in blue, green, and red color represent low, medium, and high levels of remnant polarization ($-P_r$), respectively. The hollow balls in blue, green, and red color represent low, medium, and high levels of spontaneous polarization ($-P_{max}$), respectively. (d) Plot of $-P_r$ and $-P_{max}$ as a function of external electric field. The blue, red, and green colors correspond to the three different remnant polarization states. (e) Systematic gate sweep of R_S as a function of $-P_{max}$. (f) R_S as a function of $-P_r$.

transparent (>95%) in the visible wavelength range, making them suitable for optoelectronics applications where a combination of both is required. With the excellent mechanical support of P(VDF-TrFE), the hybrid GFeTCs fabrication can also easily be integrated with industrial-scale fabrication processes such as roll-to-roll techniques. Furthermore, the limiting factors to achieve even lower sheet resistances in large-scale graphene are analyzed by means of low-temperature measurements. Our results show that, once CVD graphene synthesis and transfer processes are optimized, even lower sheet resistances are feasible without degrading the optical transparency.

RESULTS AND DISCUSSION

The device fabrication procedures of GFeTCs for sheet resistance (R_S) and optical transparency (T) measurements are illustrated in Figure 1 (for details see Methods). For R_S characterization, the device fabrication begins by patterning large-scale devices on a Si/SiO_2 substrate. After coating the P(VDF-TrFE) thin film on top of graphene, field effect transistor devices are formed by contacting them with a top gate. Their R_S as a function of P(VDF-TrFE) polarization is ready to be characterized, and the corresponding device structure is illustrated in Figure 1(iv). For T measurements and subsequent transport measurements on such transparent substrates the corresponding device diagram is shown in Figure 1(vii). Note that graphene−P(VDF-TrFE) hybrid structures can also be free-standing due to the excellent mechanical support from P(VDF-TrFE) thin films, as shown in the same figure. For large-scale application, corona poling can be used for simple, contact-free, and large-scale polarization.[33] The latter can be easily integrated with a roll-to-roll process.[16]

Figure 2a shows a wafer-scale array of large graphene field effect transistor devices on a 500 nm Si/SiO_2 substrate. In each unit cell, the graphene area is 1.44 mm^2, which is 10^6 times larger than typical CVD graphene devices (~3 μm^2).[34,35] The mobility (μ) of such large-scale devices at room temperature varies between 2000 and 4000 cm^2/(V s). Here we discuss two representative samples in detail with a mobility of ~2000 cm^2/(V s) before spin coating of P(VDF-TrFE) (see Supporting Information). The coating of the P(VDF-TrFE) dielectric is followed by the definition of top contacts; the final device structure in the van der Pauw measurement geometry is shown in Figure 2b. The mobility of both devices remains ~2000 cm^2/(V s), *i.e.*, comparable to the initial values. Figure 2c shows the typical hysteresis polarization loops of P(VDF-TrFE) thin films as a function of the applied electric field. The key parameters relating to the value of sheet resistance are the maximum polarization (P_{max}) and remnant polarization (P_r), which are recorded as a function of the electric field (Figure 2d). We start our discussion with the hole doping case. Both $-P_{max}$ and $-P_r$ increase and finally saturate with increasing applied electric field. The electrostatic doping level in graphene is $n(V_{P(VDF\text{-}TrFE)}) = \beta P_r/e$ (and $n(V_{P(VDF\text{-}TrFE)}) = \beta P_{max}/e$) for $-P_r$ (and $-P_{max}$),

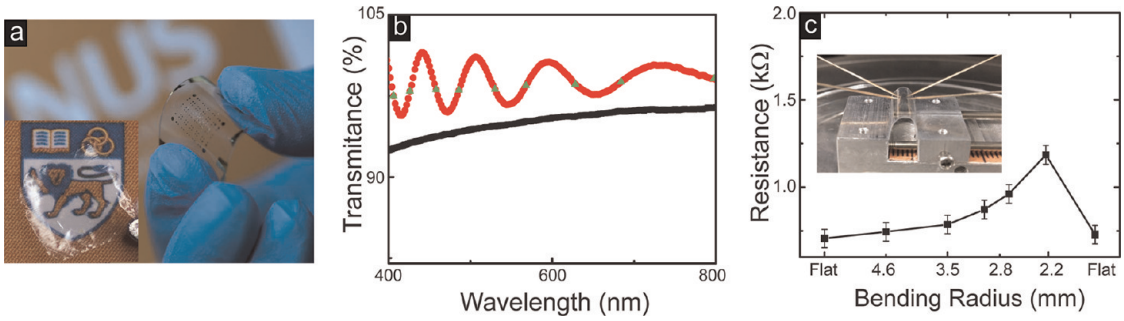

Figure 3. (a) Optical image of GFeTC samples on the transparent PET substrate. Inset shows the optical image of a free-standing graphene−P(VDF-TrFE) film held by tweezers; the background is the logo of National University of Singapore (NUS). (b) Light transmission through a graphene−P(VDF-TrFE) hybrid structure and pure P(VDF-TrFE) thin film as a function of wavelength from the visible to UV regime. The red curve shows the optical image of a pure P(VDF-TrFE) thin film. The vibration of P(VDF-TrFE) is due to the interference effect. (c) Mechanical foldability measurement of GFeTCs on a PET (200 μm) substrate. Inset shows the optical image of the four-probe bending measurement setup.

where β is the electrical coupling between ferroelectric dipoles and graphene.[26] Figure 2e and f show how R_S varies as a function of increasing $|-P_{max}|$ and $|-P_r|$, respectively. Prior to full polarization the sheet resistance of such samples is rather high (R_S = 1440 Ω/□) due to the large disorder created by randomly oriented dipoles. A 12-fold reduction of R_S is achieved only when P(VDF-TrFE) is fully polarized, resulting in a low sheet resistance of 120 Ω/□ for a single layer of graphene (Figure 2f).[36] Even lower sheet resistances could be achieved at $-P_{max}$. However, this is of little practical value, since a constant voltage needs to be applied. The key advantage of P(VDF-TrFE) is indeed that after it is fully polarized the induced nonvolatile doping allows the sheet resistance of large-scale graphene to remain low, even when the power is turned off (SFigure 3 of the Supporting Information).

Besides low sheet resistance, high optical transparency and mechanical flexibility are equally critical for the widespread application of graphene-based transparent electrodes in optoelectronics. The graphene−P(VDF-TrFE) hybrid structure for optical and electromechanical measurements is shown in Figure 3. Figure 3a shows the GFeTCs on top of PET substrates. The P(VDF-TrFE) film used here is only 1 μm thick and yet already sufficient to provide an excellent mechanical support for graphene (inset of Figure 3a). The transmission spectra as a function of wavelength from the visible to near IR are shown in Figure 3b. For a P(VDF-TrFE) thin film alone without graphene, interference effects lead to an oscillating transmittance feature.[37] Such interference effects imply a uniform P(VDF-TrFE) thin film. From the periodicity, the thickness of the P(VDF-TrFE) thin film can also be deduced to be around 1 μm. This is in good agreement with independent surface profile measurements. On the other hand, once graphene is transferred on P(VDF-TrFE) films, the interference effect vanishes and a monotonic transmittance as a function of wavelength is observed. In the visible range the optical transparency of the graphene−P(VDF-TrFE) hybrid structure ranges from 92.5% to 96.3% with 95% at 550 nm.

Next we discuss the mechanical properties of GFeTCs. Figure 3c shows the evaluation of GFeTCs' foldability on a PET substrate by measuring the resistance of graphene with respect to bending radius. The resistance showed a small increase down to the bending radius of 3.0 mm, which was recovered completely after unbending the GFeTC device. Notably, the original resistance is repeatedly restored even after bending the sample down to 1.0 mm in radius (approximate tensile strain of 11%). These outstanding mechanical properties of graphene−P(VDF-TrFE) films are comparable with the results obtained for graphene films on PET.[10]

Temperature-dependent sheet resistance measurements of large-scale CVD graphene at different doping levels were carried out to investigate the factors preventing even lower R_S. A clear transition from insulating behavior at low doping (before polarizing P(VDF-TrFE)) to metallic behavior at high doping (after fully polarizing P(VDF-TrFE)) was observed (Figure 4a). For samples of comparable mobility, previously such a behavior has been associated with a large inhomogeneity of CVD graphene specific charged impurities.[38,39] More relevant for our purpose are temperature-dependent resistivity measurements at high doping levels. At 50 K, once the phonon contribution has been eliminated (ΔR = 30 Ω/□), a residual sheet resistance of 100 Ω/□ is observed. This clearly shows that at high doping much lower sheet resistances can be achieved once CVD graphene specific charged impurities mainly due to the etching and transfer processes are reduced or eliminated.[40] Note also that high doping experiments with exfoliated graphene samples allow sheet resistances as low as 30 Ω/□ at 50 K.[41]

We can better understand our results by calculating the sheet resistance as a function of carrier density with $R_S = R_0 + R_{AP} + R_{FP}$. Here R_0 represents the residual sheet resistance due to extrinsic scattering sources,[42,43]

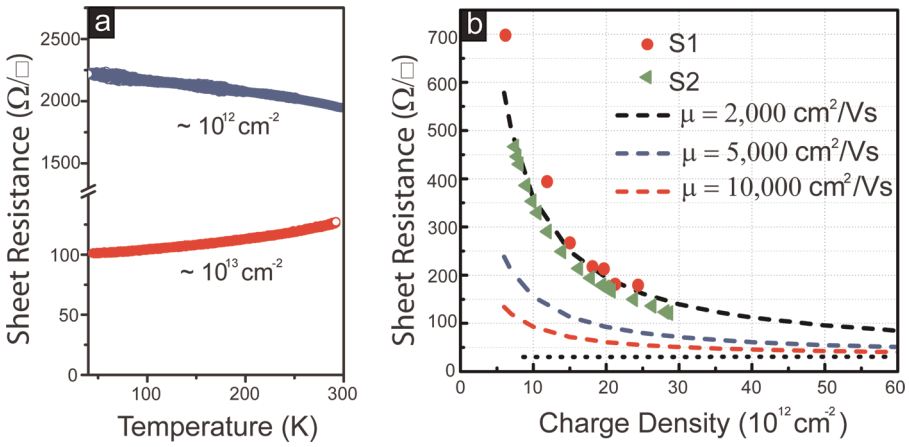

Figure 4. (a) Temperature-dependence measurements of GFeTCs at different charge density levels. The blue solid curve indicates the insulating behavior of GFeTCs at low density level; the red solid curve indicates the metallic behavior of GFeTC at high density level. (b) Experimental data and theoretical estimations of R_S as a function of μ and n.

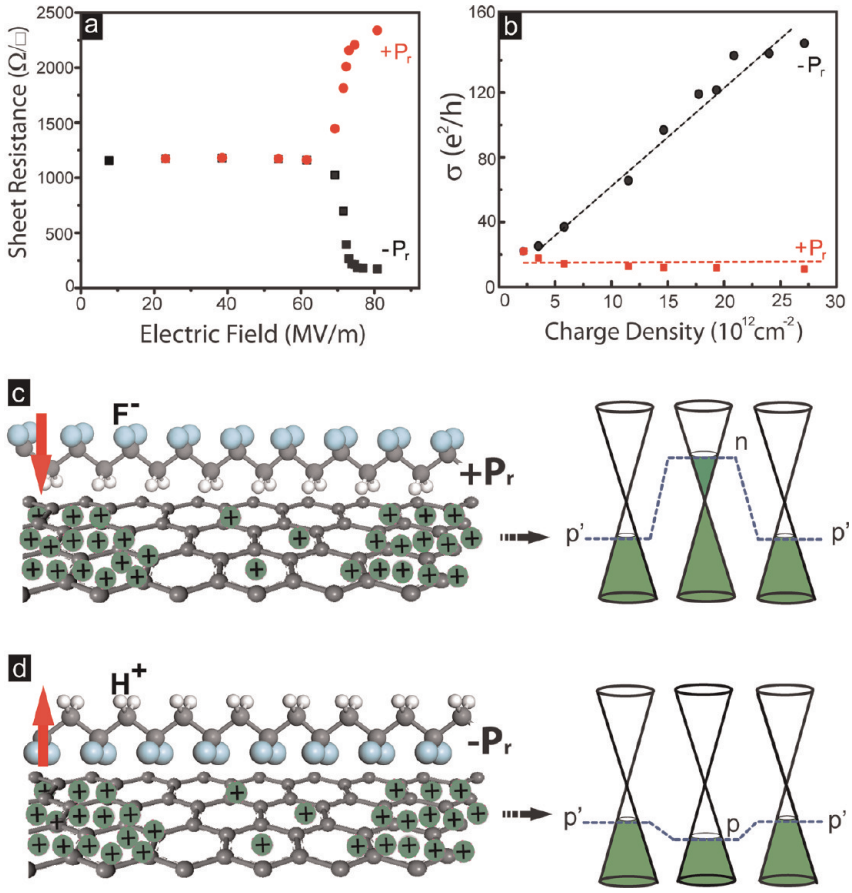

Figure 5. (a) R_S as a function of both $+P_r$ and $-P_r$. (b) The corresponding conductivity as a function of both $+P_r$ and $-P_r$. (c) Electrostatic doping in graphene with P(VDF-TrFE) at the $+P_r$ state. The green particles in graphene represent the initial p-type charged impurities doping. After fully polarizing the ferroelectric thin film, the formation of n−p electron−hole puddles in graphene explains the results observed in (a) and (b). (d) Electrostatic doping in graphene with P(VDF-TrFE) at the $-P_r$ state.

the acoustic phonon scattering R_{AP} gives rise to a linear T-dependent resistivity,[44] and $R_{FP} \approx T^2/(n/10^{12} + \gamma)$ represents the contributions from flexural phonons.[45] Using this formula, R_S *vs* n can be plotted for mobilities ranging from 2000 to 10 000 cm^2/(V s). With this we can now compare the R_S values obtained at different n for two different samples (Figure 4b). For both samples the experimental data can be well explained, if one assumes $\mu \approx 2000$ cm^2/(V s). Since this value is comparable to the device mobility before the spin-coating of

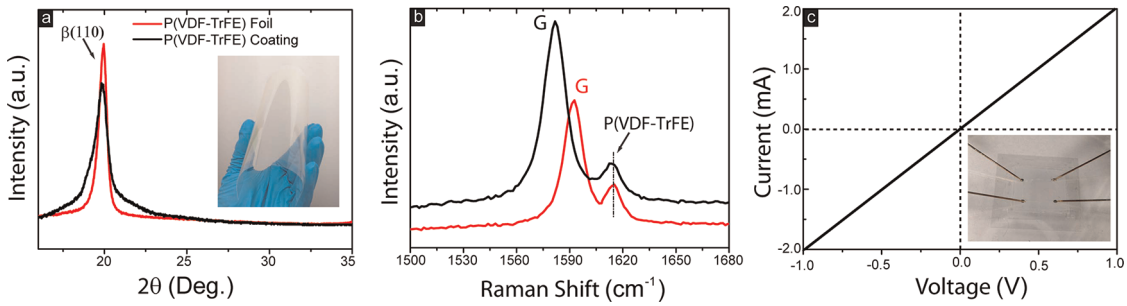

Figure 6. (a) XRD results of both P(VDF-TrFE) foil and house-produced P(VDF-TrFE) film. Inset shows the optical image of large-scale prepolarized P(VDF-TrFE) foil on a PET substrate. (b) Raman spectra of graphene on unpolarized (black) and prepolarized (red) P(VDF-TrFE) foils. For clarity, we focus on the graphene G peak shift from 1580 cm^{-1} (unpolarized) to 1592 cm^{-1} (prepolarized) as a comparison of the doping effect from P(VDF-TrFE) foil. (c) $I-V$ characterization of the sheet resistance of large-scale graphene on the prepolarized P(VDF-TrFE) foil. Inset shows the device characterization image.

the ferroelectric polymer (~2300 $cm^2/(V\ s)$), we conclude that the latter is currently not limited by the small content of nonferroelectric phase in P(VDF-TrFE).[26] Last but not least, we further estimate R_S for high-mobility samples at room temperature. As expected, the sheet resistance decreases with increasing mobility and can reach for realistic device mobilities of 10 000 $cm^2/(V\ s)$ low values of 50 Ω/□ at 3×10^{13} cm^{-2}. Note also that, at least at room temperature high doping may avoid the need for combining graphene with BN; even a doubling of the device mobility to 20 000 $cm^2/(V\ s)$ would reduce only marginally the sheet resistance any further.[46,47]

The presence of a large inhomogenous background doping in large-scale GFeTCs becomes even more evident in R_S *vs* $+P_r$ measurements (Figure 5a). Compared to a monotonic decrease of R_S with $-P_r$, a continuous increase of R_S with increasing $+P_r$ is observed instead. Note that also the corresponding μ differs strongly at $-P_r$ and $+P_r$, as shown in Figure 5b. Such a strong asymmetry in both R_S and μ is observed only in mm^2 size large-scale samples and absent in our μm^2 size devices. This implies the existence of a nonuniform p-type background doping in large-scale CVD graphene after transfer. A simple model sketched in Figure 5c, d illustrates this scenario. When ferroelectric dipoles are tuned to be $+P_r$, the corresponding electrostatic n-type doping in graphene gives rise to a random array of p−n junctions, resulting in large potential steps along the current path (Figure 5c). As a consequence, sheet resistance is strongly enhanced. On the other hand, for $-P_r$ we obtain p−p′ junctions (Figure 5d), leading to a much smoother potential landscape and, hence, a much lower sheet resistance.

For large-scale applications, the lamination of CVD graphene with commercially available prepolarized P(VDF-TrFE) foils is more intriguing. Utilizing such foils, low sheet resistances of large-scale graphene can be immediately achieved without further ferroelectric poling. This can largely simplify the device fabrication steps. Figure 6a shows the XRD measurements of both prepolarized P(VDF-TrFE) foil and in-house-produced P(VDF-TrFE) thin film. Both show a pronounced diffraction peak, which clearly indicates that the ferroelectric phase (β-phase) is highly crystalline.[48] The doping induced on graphene by the unpolarized and prepolarized P(VDF-TrFE) foils is further determined by the Raman spectroscopy measurements (Figure 6b). For graphene on prepolarized P(VDF-TrFE) foil, a G peak shift of around 12 cm^{-1} is observed, corresponding to ~1×10^{13} cm^{-1} electron doping.[49] At this doping level, the $I-V$ measurements yields a sheet resistance value of ~500 Ω/□ (Figure 6c). This value, while ~5 times larger than what has been achieved with in-house-produced P(VDF-TrFE), is promising, since the results can be further improved by optimizing the remnant polarization of commercial P(VDF-TrFE) sheets and the graphene on P(VDF-TrFE) transfer process and by graphene/P(VDF-TrFE) interface engineering (see Supporting Information). Equally important, both n-type- and p-type-doped graphene films can be realized by transferring them to either side of prepolarized P(VDF-TrFE) foils. Such graphene films can, for example, in principle directly serve as anode and cathode in photovoltaic devices with controllable polarity.[26] For instance, the realization of n-type-doped graphene is attractive for low work function cathode in light-emitting diodes and solar cell devices.[50]

CONCLUSIONS

In conclusion, we have demonstrated a new type of transparent conductor using graphene−ferroelectric hybrid films. The ferroelectric thin film does not compromise the high optical transparency of graphene. It provides *nonvolatile* electrostatic doping, yielding even in low mobility samples a sheet resistance as low as 120 Ω/□. The ferroelectric polymer also serves as an excellent mechanical supporting layer, making GFeTCs easily transferable and integrable with flexible electronics, optoelectronics, and photonics platforms. In addition, we show that the limiting factors for further lowering the sheet resistance are not the ferroelectric polymer but commonly known charged impurities

originating from existing transfer processes. Therefore, with further improvements in the transfer process a sheet resistance of 50 Ω/□ at an optical transparency of >95% seems feasible.

METHODS

Device Fabrications. Device fabrication begins with the large-scale graphene synthesized by the CVD method on pure copper foils (Figure 1(i)), the details of graphene fabrication procedures are discussed in refs 11 and 16. For the sheet resistance measurements, GFeTC devices are fabricated on conventional Si/SiO_2 (500 and 300 nm) substrates as shown from Figure 1(ii) to (iv). (ii) The Cu-CVD graphene was immersed into a copper etchant. (iii) Once the copper was etched away, the large-scale graphene was immediately transferred onto the substrates followed by standard e-beam lithography and an oxygen plasma etching process to separate large-scale graphene sheets into 1.2 mm by 1.2 mm graphene squares. After this, metal contacts (5 nm Cr/30 nm Au) were defined using the predefined shielding mask followed by a thermal evaporation process. The devices were further thermally annealed at 250 °C in H_2/Ar conditions for 3 h. (iv) After spin coating 1.0 μm thick poly(vinylidene fluoride-trifluoroethylene) (P(VDF-TrFE)) followed by thermally evaporating the top gate electrodes, samples were ready to be characterized.

Figure 1(v) to (vii) summarizes the GFeTC devices for the optical transparency measurements. (v) The P(VDF-TrFE) thin film was spin-coated directly on top of graphene, which serves as the dielectric as well as mechanical supporting layer in the following steps. (vi) The Cu-CVD graphene−P(VDF-TrFE) structure was immersed into copper etchant. (vii) After removing the copper and rinsing in DI water, the graphene−P(VDF-TrFE) hybrid structure was immediately transferred to transparent substrates, *i.e.*, PET or glass substrates. For the optical measurements, the transparency of graphene−P(VDF-TrFE) *vs* wavelength is characterized using a UV Probe 3600 at ambient conditions. The incident power intensity is 5000 mW.

Transport Measurements. Transport measurements were electrically characterized in ambient conditions with a standard van der Pauw configuration using a lock-in amplifier with an excitation current of 100 nA. In total six single-layer large-scale graphene devices have been measured. Here we discuss two representative SLG devices in more detail. For the temperature-dependent measurements, samples were characterized in a variable-temperature insert in a liquid helium cryostat ($T = 2-300$ K).

To polarize the ferroelectric thin film, we mainly utilized the ferroelectric Radiant polarizer, which injects a voltage pulse either positive or negative into the top gate electrode. After this, the corresponding resistivity of large-scale graphene at each P_r magnitude of ferroelectric thin film was recorded using the van der Pauw approach, as shown in Figure 2f. Note that for the van der Pauw measurements, the horizontal direction resistivities and vertical direction resistivities were first compared to make sure their differences are negligible. Then the sheet resistance is calculated using the standard formula ($R_S = \pi R/\ln 2 \approx 4.53R$).

Optical Measurements. The linear optical transparency was measured using the UV−vis−NIR spectrophotometer. The spectra are collected in a 1.0 mm path length cell. To perform these measurements, the graphene/ferroelectric hybrid structures are transferred to a glass substrate.

Raman Spectroscopy. Raman spectroscopy/imaging were carried out with a WITEC CRM200 Raman system with 532 nm (2.33 eV) excitation and laser power at sample below 0.1 mW to avoid laser-induced heating. A 50× objective lens with a NA = 0.95 was used in the Raman experiments. Data analysis was done using WITec Project software.

XRD Measurements. The model of the XRD setup is Bruker Discover D8; the X-ray source, Cu Kα line (λ =1.541838 Å).

Conflict of Interest: The authors declare no competing financial interest.

Acknowledgment. The authors gratefully acknowledge Natarajan Chandrasekhar, Cedric Troadec, Yuda Ho, Chee-Tat Toh, and Amar Srivastava for their help with the device preparations. This work is supported by the Singapore National Research Foundation [grants NRF-RF2008-07, NRF-CRP(R-144-000-295-281), NRF-POC002-038, NUS-YIA(R144-000-283-101), IMRE/10-1C0109, and NUS/SMF], U.S. Office of Naval Research (ONR and ONR Global), A*STAR SERC TSRP-Integrated Nano-photo-Bio Interface (R-144-000-275-305), NUS NanoCore, and the National Research Foundation of Korea (NRF) funded by the Ministry of Education, Science and Technology (Global Research Lab. 20110021972, 2011K000615, 20110017587, 20110006268, and Global Frontier Research Program 20110031629).

Supporting Information Available: (1) Electrical transport characterization of large-scale CVD graphene. (2) Graphene device fabrication on commercially available prepolarized P-(VDF-TrFE) sheets. (3) Retention characterization. This information is available free of charge *via* the Internet at http://pubs.acs.org.

REFERENCES AND NOTES

1. Geim, A. K. Graphene: Status and Prospects. *Science* **2009**, *324*, 1530–1534.
2. Castro Neto, A. H.; Guinea, F.; Peres, N. M. R.; Novoselov, K. S.; Geim, A. K. The Electronic Properties of Graphene. *Rev. Mod. Phys.* **2009**, *81*, 109–162.
3. Novoselov, K. S.; Geim, A. K.; Morozov, S. V.; Jiang, D.; Zhang, Y.; Dubonos, S. V.; Grigorieva, I. V.; Firsov, A. A. Electric Field Effect in Atomically Thin Carbon Films. *Science* **2004**, *306*, 666–669.
4. Zhang, Y.; Tan, J. W.; Stormer, H. L.; Kim, P. Experimental Observation of the Quantum Hall Effect and Berry's Phase in Graphene. *Nature* **2005**, *438*, 201–204.
5. Nair, R. R.; Blake, P.; Grigorenko, A. N.; Novoselov, K. S.; Booth, T. J.; Stauber, T.; Peres, N. M. R.; Geim, A. K. Fine Structure Constant Defines Visual Transparency of Graphene. *Science* **2008**, *320*, 1308.
6. Lee, C.; Wei, X.; Kysar, J. W.; Hone, J. Measurement of the Elastic Properties and Intrinsic Strength of Monolayer Graphene. *Science* **2008**, *321*, 385–388.
7. Avouris, P. Graphene: Electronic and Photonic Properties and Devices. *Nano Lett.* **2010**, *10*, 4285–4294.
8. Bonaccorso, F.; Sun, Z.; Hasan, T.; Ferrari, A. C. Graphene Photonics and Optoelectronics. *Nat. Photonics* **2010**, *4*, 611–622.
9. Wang, F.; Zhang, Y. B.; Tian, C. S.; Girit, C.; Zettl, A.; Crommie, M.; Shen, Y. R. Gate-Variable Optical Transitions in Graphene. *Science* **2008**, *320*, 206–209.
10. Kim, K. S.; Zhao, Y.; Jang, H.; Lee, S. Y.; Kim, J. M.; Kim, K. S.; Ahn, J. H.; Kim, P.; Choi, J. Y.; Hong, B. H. Large-Scale Pattern Growth of Graphene Films for Stretchable Transparent Electrodes. *Nature* **2009**, *457*, 706–710.
11. Li, X. S.; Cai, W. W.; An, J.; Kim, S.; Nah, J.; Yang, D. X.; Piner, R.; Velamakanni, A.; Jung, I.; Tutuc, E.; Banerjee, S. K.; *et al.* Large Area Synthesis of High-Quality and Uniform Graphene Films on Copper Foils. *Science* **2009**, *324*, 1312–1314.
12. Wang, X.; Zhi, L. J.; Mullen, K. Transparent, Conductive Graphene Electrodes for Dye-Sensitized Solar Cells. *Nano Lett.* **2007**, *8*, 323–327.
13. Wu, J. B.; Agrawal, M.; Becerril, H. A.; Bao, Z. N.; Liu, Z. F.; Chen, Y. S.; Peumans, P. Organic Light-Emitting Diodes on Solution-Processed Graphene Transparent Electrodes. *ACS Nano* **2010**, *4*, 43–48.
14. Blake, P.; Brimicombe, P. D.; Nair, R. R.; Booth, T. J.; Jiang, D.; Schedin, F.; Ponomarenko, L. A.; Morozov, S. V.; Gleeson, H. F.; Hill, E. W.; *et al.* Graphene-Based Liquid Crystal Device. *Nano Lett.* **2008**, *8*, 1704–1708.
15. Gordon, R. G. Criteria for Choosing Transparent Conductors. *MRS Bull.* **2000**, *25*, 52–57.

16. Bae, S.; Kim, H.; Lee, Y.; Xu, X.; Park, J. S.; Zheng, Y.; Balakrishnan, J.; Lei, T.; Kim, H. R.; Song, Y.; *et al*. Roll-to-Roll Production of 30-Inch Graphene Films for Transparent Electrodes. *Nat. Nanotechnol.* **2010**, *5*, 574–578.
17. Gunes, F.; Shin, H. J.; Biswas, C.; Han, H. G.; Kim, E. S.; Chae, S. J.; Choi, J. R.; Lee, Y. H. Layer by Layer Doping of Few Layer Graphene Film. *ACS Nano* **2009**, *4*, 4595–4600.
18. Kasry, A.; Kuroda, M. A.; Martyna, G. J.; Tulevski, G. S.; Bol, A. A. Chemical Doping of Large-Area Stacked Graphene Films for Use as Transparent, Conducting Electrodes. *ACS Nano* **2010**, *4*, 3839–3844.
19. Xie, L. F.; Wang, X.; Mao, H.; Wang, R.; Ding, M.; Wang, Y.; Özyilmaz, B.; Loh, K. P.; Wee, A. T. S.; Ariando; *et al*. Electrical Measurement of Non-Destructively P-type Doped Graphene Using Molybdenum Trioxide. *Appl. Phys. Lett.* **2011**, *99*, 012112.
20. Liu, H. T.; Liu, Y. Q.; Zhu, D. B. Chemical Doping of Graphene. *J. Mater. Chem* **2011**, *21*, 3335–3345.
21. Wehling, T. O.; Novoselov, K. S.; Morozov, S. V.; Vdovin, E. E.; Katsnelson, M. I.; Geim, A. K.; Lichtenstein, A. I. Molecular Doping of Graphene. *Nano Lett.* **2008**, *8*, 173–177.
22. Lee, B.; Chen, Y.; Duerr, F.; Mastrogiovanni, D.; Garfunkel, E.; Andrei, E. Y.; Podzorov, V. Modification of Electronic Properties of Graphene with Self-Assembled Monolayers. *Nano Lett.* **2010**, *10*, 2427–2432.
23. Chandra, B.; Afzali, A.; Khare, N.; El-Ashry, M. M.; Tulevski, G. S. Stable Charge-Transfer Doping of Transparent Single-Walled Carbon Nanotube Films. *Chem. Mater.* **2010**, *22*, 5179–5183.
24. Yan, C.; Kim, K. S.; Lee, S. K.; Bae, S. H.; Hong, B. H.; Kim, J. H.; Kim, J. H.; Lee, H. J.; Ahn, J. H. Mechanical and Environmental Stability of Polymer Thin Film Coated Graphene. *ACS Nano* **2012**, *6*, 2096–2103.
25. Hu, Z.; Tian, M.; Nysten, B.; Jonas, A. M. Regular Arrays of Highly Ordered Ferroelectric Polymer Nanostructures for Non-Volatile Low-Voltage Memories. *Nat. Mater.* **2008**, *8*, 62–67.
26. Zheng, Y.; Ni, G. X.; Toh, C. T.; Tan, C. Y.; Yao, K.; Özyilmaz, B. Graphene Field-Effect Transistors with Ferroelectric Gating. *Phys. Rev. Lett.* **2010**, *105*, 166602.
27. Zheng, Y.; Ni, G. X.; Toh, C. T.; Zeng, M. G.; Chen, S. T.; Yao, K.; Özyilmaz, B. Gate-Controlled Non-Volatile Graphene-Ferroelectric Memory. *Appl. Phys. Lett.* **2009**, *94*, 163505.
28. Yuan, Y.; Reece, T. J.; Sharma, P.; Poddar, S.; Ducharme, S.; Gruverman, A.; Yang, Y.; Huang, J. Efficiency Enhancement in Organic Solar Cells with Ferroelectric Polymers. *Nat. Mater.* **2011**, *10*, 296–302.
29. Yao, K.; Chen, S.; Rahimabady, M.; Mirshekarloo, M. S.; Yu, S.; Tay, F. E. H.; Sritharan, T.; Lu, L. Nonlinear Dielectric Thin Films for High-Power Electric Storage with Energy Density Comparable with Electrochemical Supercapacitors. *IEEE Trans. Ultrason. Ferroelectrics Freq. Contr.* **2011**, *58*, 1968–1974.
30. Bierwagen, G.; Shedlosky, T. J.; Stanek, K. Developing and Testing a New Generation of Protective Coatings for Outdoor Bronze Sculpture. *Prog. Org. Coat.* **2003**, *48*, 289–296.
31. Nalwa, H. S. *Ferroelectric Polymers Chemistry, Physics, and Applications*; CRC Press, 1995.
32. Lee, W. H.; Suk, J. W.; Lee, J.; Hao, Y.; Park, J.; Yang, J. W.; Ha, H. W.; Murali, S.; Chou, H.; Akinwande, D.; *et al*. Simultaneous Transfer and Doping of CVD-Grown Graphene by Fluoropolymer for Transparent Conductive Films on Plastic. *ACS Nano* **2012**, *6*, 1284–1290.
33. Kaura, T.; Nath, R.; Perlman, M. M. Simultaneous Stretching and Corona Poling of PVDF Films. *J. Phys. D: Appl. Phys.* **1991**, *24*, 1848–1852.
34. Ni, G. X.; Zheng, Y.; Bae, S.; Kim, H. R.; Pachoud, A.; Kim, Y. S.; Tan, C. L.; Im, D.; Ahn, J. H.; Hong, B. H.; *et al*. Quasi-Periodic Nanoripples in Graphene Grown by Chemical Vapor Deposition and Its Impact on Charge Transport. *ACS Nano* **2012**, *6*, 1158–1164.
35. Zheng, Y.; Ni, G. X.; Bae, S.; Cong, C. X.; Kahya, O.; Toh, C. T.; Kim, H. R.; Im, D.; Yu, T.; Ahn, J. H.; *et al*. Wafer-Scale Graphene/Ferroelectric Hybrid Devices for Low-Voltage Electronics. *Europhys. Lett.* **2011**, *93*, 17002.
36. Here, the electrostatic doping level is obtained using $\sigma = n_{(VP(VDF-TrFE))}e\mu$ under the assumption that the charge carrier density is constant, which is supported from our R *vs* V_{BG} measurements.
37. Swanepoel, R. Determine of the Thickness and Optical Constants of Amorphous Silicon. *J. Phys. E: Sci. Instrum.* **1983**, *16*, 1214–1222.
38. Heo, J.; Chung, H. J.; Lee, S. H.; Yang, H.; Seo, D. H.; Shin, J. K.; Chung, U. I.; Seo, S.; Hwang, E. H.; Sarma, S. D. Nonmonotonics Temperature Dependent Transport in Graphene Grown by Chemical Vapor Deposition. *Phys. Rev. B* **2010**, *84*, 035421.
39. Ferreira, A.; Xu, X. F.; Tan, C. L.; Bae, S. K.; Peres, N. M. R.; Hong, B. H.; Özyilmaz, B.; Castro Neto, A. H. Transport Properties of Graphene with One-Dimensional Charge Defects. *Europhys. Lett.* **2011**, *94*, 28003.
40. Note that such high electrostatic doping also strongly suppresses flexural phonon scattering due to the presence of nanoripple arrays in CVD graphene.[34]
41. Efetov, D. K.; Kim, P. Controlling Electron-Phonon Interactions in Graphene at Ultrahigh Carrier Densities. *Phys. Rev. Lett.* **2010**, *105*, 256805.
42. Chen, J. H.; Jang, C.; Xiao, S. D.; Ishigami, M.; Fuhrer, M. S. Intrinsic and Extrinsic Performance Limits of Graphene Devices on SiO_2. *Nat. Nanotechnol.* **2008**, *3*, 206–209.
43. Wehling, T. O.; Yuan, S.; Lichtenstein, A. I.; Geim, A. K.; Katsnelson, M. I. Resonant Scattering by Realistic Impurities in Graphene. *Phys. Rev. Lett.* **2010**, *105*, 056802.
44. Hwang, E. H.; Sarma, S. D. Acoustic Phonon Scattering Limited Carrier Mobility in Two Dimensional Extrinsic Graphene. *Phys. Rev. B* **2008**, *77*, 115449.
45. Castro, E. V.; Ochoa, H.; Katsnelson, M. I.; Gorbachev, R. V.; Elias, D. C.; Novoselov, K. S.; Geim, A. K.; Guinea, F. Limits on Electron Quality in Suspended Graphene Due to Flexural Phonons. *Phys. Rev. Lett.* **2010**, *105*, 266601.
46. Ducharme, S.; Reece, J. T.; Othon, C. M.; Rannow, R. K. Ferroelectric Polymer Langmuir–Blodgett Films for Nonvolatile Memory Applications. *IEEE Trans. Electron Devices* **2005**, *5*, 720–735.
47. Gannett, W.; Regan, W.; Watanabe, K.; Taniguchi, T.; Crommie, M. F.; Zettl, A. Boron Nitride Substrates for High Mobility Chemical Vapor Deposited Graphene. *Appl. Phys. Lett.* **2011**, *98*, 242105.
48. Chen, S. T.; Yao, K.; Tay, F. E. H.; Chew, L. L. S. Comparative Investigation of the Structure and Properties of Ferroelectric Poly(vinylidene fluoride) and Poly(vinylidene fluoride–trifluoroethylene) Thin Films Crystallized on Substrates. *J. Appl. Polym. Sci.* **2010**, *116*, 3331–3337.
49. Das, A.; Pisana, S.; Chakraborty, B.; Piscanec, S.; Saha, S. K.; Waghmare, U. V.; Novoselov, K. S.; Krishnamurthy, H. R.; Geim, A. K.; Ferrari, A. C.; *et al*. Monitoring Dopants by Raman Scattering in an Electrochemically Top-Gated Graphene Transistor. *Nat. Nanotechnol.* **2008**, *3*, 210–215.
50. Hwang, J. O.; Park, J. S.; Choi, D. S.; Kim, J. Y.; Lee, S. H.; Lee, K. E.; Kim, Y. H.; Song, M. H.; Yoo, S.; Kim, S. O. Workfunction-Tunable, N-Doped Reduced Graphene Transparent Electrodes for High-Performance Polymer Light-Emitting Diodes. *ACS Nano* **2012**, *6*, 159–167.